PHYSICAL REVIEW B **87**, 085207 (2013)

Evidence for space-charge-limited conduction in organic photovoltaic cells at open-circuit conditions

Daniele Di Nuzzo, Stephan van Reenen, René A. J. Janssen, Martijn Kemerink, and Stefan C. J. Meskers*
Molecular Materials and Nanosystems, Technical University Eindhoven, PO Box 530, NL-5600MB, The Netherlands
(Received 20 November 2012; published 28 February 2013)

The ac admittance of solar cells under illumination is investigated under open-circuit conditions. Open-circuit conditions are imposed by inserting a probe capacitor into the circuit. The capacitance and conductance of the cells are investigated as function of frequency and continuous illumination intensity. Results are compared with numerical and analytical modeling of charge recombination and transport. In bulk heterojunction solar cells with [6,6]-Phenyl-$C_{61}(C_{71})$-butyric acid methyl ester as acceptor and poly(3-hexylthiophene) or poly[2-methoxy-5-(2′-ethylhexyloxy)-p-phenylene vinylene] as electron donor, the high-frequency capacitance C and conductance G follow a power-law dependence on intensity of white light I, with $G(I) \propto I^{3/4}$ and $C(I) \propto I^{1/4}$. The modeling shows that these dependencies can be explained in terms of space-charge-limited current in combination with Langevin type recombination of carriers. For poly[2,1,3-benzothiadiazole-4,7-diyl[4,4-bis(2-ethylhexyl)-4H-cyclopenta[2,1-b:3,4-b′]dithiophene-2,6-diyl]] the capacitance shows a weaker dependence on intensity, indicating fast recombination of photogenerated carriers. Results indicate that the fill factor of relatively well performing polymer solar cells can still be limited by space charge effects and can be improved by enhancing the charge carrier mobility or by reducing the bimolecular Langevin recombination.

DOI: 10.1103/PhysRevB.87.085207 PACS number(s): 73.61.Ph, 78.20.Jq, 85.60.−q

I. INTRODUCTION

Compared to cells made of inorganic semiconductors, polymer solar cells show lower efficiencies ($\leqslant 11\%$).[1–7] Part of the lower efficiency is due to a relatively poor fill factor (FF), defined as the ratio of the maximum extractable power and the product of short-circuit current (J_{sc}) and open-circuit voltage (V_{oc}). In solar cells with high fill factors the photocurrent $|J|$ shows a steplike, sharp drop for voltages approaching the open-circuit potential V_{oc}. This implies a large value of the conductance $G = dJ/dV$ at voltages near V_{oc} for solar cells with high fill factor.

In order to improve the fill factor in a rational way, it is mandatory to have an understanding of which processes limit the current densities in polymer solar cells near open-circuit conditions and thus control the conductance of the cell. In scientific literature on polymer solar cells, various possible limiting factors on the photocurrent near V_{oc} have been discussed.

First, the current may be limited by the rate of charge generation. In polymer solar cells efficient generation of extractable charge carriers from primary photoexcitations can be realized, but is found to be strongly dependent on materials and processing conditions used.[8] Near V_{oc}, where the internal electric field in the cell is small, charge generation may be low because of a field dependence of the generation process of mobile carriers out of the primary photoexcitations as indicated by modeling of photocurrents.[9] Furthermore, primary photoexcitations may decay rapidly due to the close proximity of charge carriers in the material (exciton-charge annihilation). Exciton-charge annihilation is likely to reduce the overall generation efficiency near V_{oc}, because carrier densities increase when going from short-circuit to open-circuit conditions. Second, currents may be limited due to rapid recombination of photogenerated charge carriers. This recombination may be of Langevin type,[10] but could also be effected by the metal contacts.[11] Third, currents may also be limited by space charge effects. The net amount of charge that can be accumulated in a certain volume of semiconducting material is restricted because of the electrostatic energy needed to build up such a space charge and generally depends on the potential difference over the semiconducting layer.[12,13] It is important to realize that the possible sources of current limitation discussed above are not mutually exclusive. For instance, a space-charge limitation on current densities automatically implies *some sort* of recombination in the bulk of the device.

Here we investigate the (photo-)admittance of polymer:fullerene bulk heterojunction solar cells in order to develop an understanding of the limiting processes in the photocurrent generation in the solar cells near open-circuit conditions. The polymers poly(3-hexylthiophene) (P3HT), poly[2,1,3-benzothiadiazole-4,7-diyl[4,4-bis(2-ethylhexyl)-4H-cyclopenta[2,1-b:3,4-b′]dithiophene-2,6-diyl]] (PCPDTBT), and poly[2-methoxy-5-(2′-ethylhexyloxy)-p-phenylene vinylene] (MDMO-PPV) (Fig. 1) are used as electron donors in the bulk heterojunctions with either [6,6]-Phenyl-$C_{61}(C_{71})$-butyric acid methyl ester ([60]PCBM or [70]PCBM) as electron acceptor.

Realizing open-circuit conditions in a conduction experiment can be complicated. We overcome this difficulty by inserting a probe capacitor in the analysis circuit. In this way one can automatically ensure open-circuit conditions under all continuous, white light illumination intensities (Fig. 2). Since no dc signals can be present in this configuration, ac analysis is necessary: applying a small oscillating ac bias voltage, the conductance and capacitance of the cell can be probed as function of frequency and illumination intensity.[14–16]

Experimental investigations are combined with numerical and analytical modeling of photocurrents under open-circuit conditions considering drift and diffusion transport in combination with Langevin-type bimolecular recombination of charge carriers. We find that the dependence of photoconductance G on illumination intensity I can be described by $G(I) \propto I^{3/4}$ while the photocapacitance C follows $C(I) \propto I^{1/4}$. We attribute this common behavior to a space-charge limitation on the magnitude of the photocurrent in the polymer:fullerene

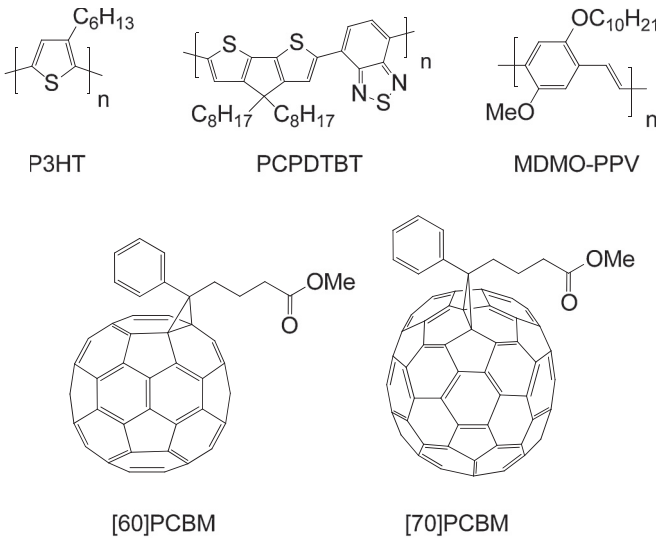

FIG. 1. Chemical structure of the materials used.

bulk heterojunction layer of the cells under the open-circuit-like conditions that we impose.

II. EXPERIMENT

A. Materials and device fabrication

Photovoltaic devices were made by spin coating poly(ethylenedioxythiophene):poly(styrene sulfonate) (PEDOT:PSS) (Clevios P, VP Al4083) onto precleaned, patterned indium tin oxide (ITO) substrates (14 Ω per square) (Naranjo Substrates). [6,6]-Phenyl-$C_{61}(C_{71})$-butyric acid methyl ester ([60]([70])PCBM) (Solenne) was used as electron acceptor in spin-coated bulk heterojunction active layers in combination with π-conjugated polymers as electron donors. The bulk heterojunction layers were deposited by spin coating in air at room temperature. Below the specific fabrication procedure for each conjugated polymer used is listed.

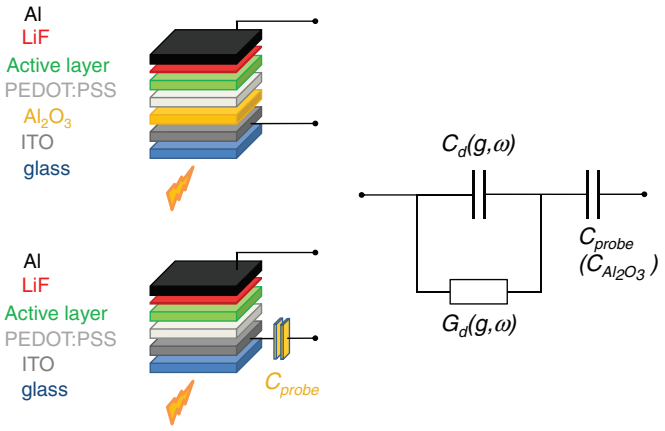

FIG. 2. (Color online) (left top) Layout of the device used in the impedance spectroscopy on P3HT:[60]PCBM based solar cells including an insulating layer (Al_2O_3). (left bottom) Alternatively, an external probe (C_{probe}) capacitor was connected in series to a standard solar cell. Both devices can be represented by the equivalent circuit at the right.

Poly[3-hexylthiophene] (P3HT) (M_n < 50 kg/mol, 98% regioregular, Rieke) was spin coated at 5000 rpm from chloroform:chlorobenzene (1:1 volume) solution containing 15 mg P3HT per mL and [60]PCBM in a 1:1 polymer:[60]PCBM weight ratio. Both as cast and thermally annealed devices were fabricated. Annealing was performed at 140 °C for 60 s in inert atmosphere prior to the metal electrode evaporation. Active layer thickness = 70 nm. Modified P3HT:[60]PCBM devices were also fabricated, incorporating a 30-nm Al_2O_3 layer deposited by means of atomic layer deposition (ALD) on top of ITO and before spin coating PEDOT:PSS and the active layer. The devices incorporating Al_2O_3 combined with an active bulk heterojunction layer of 70-nm thick were not annealed.

Poly(2-methoxy-5-(3,7-dimethyloctyloxy)-1,4-phenylene vinylene) (MDMO-PPV) ($M_w \approx 10^3$ kg/mol, PDI = 7) was spin coated at 1000 rpm using a chlorobenzene solution containing 3 mg MDMO-PPV per mL and [60]PCBM in a 1:4 polymer:[70]PCBM weight ratio. Active layer thickness = 175 nm.

Poly[2,6-(4,4-bis(2-ethylhexyl)-4H-cyclopenta [2,1-b;3,4-b0]dithiophene)-alt-4,7-(2,1,3-benzothiadiazole (PCPDTBT) (M_n = 27.7 kg/mol, PDI = 1.9) was spin coated at 2000 rpm using a chlorobenzene solution containing 10 mg of PCPDTBT per mL and [70]PCBM in a 1:2 polymer:[70]PCBM weight ratio. Active layer thickness = 80 nm. Note that the morphology for this bulk heterojunction has not been optimized using cosolvent.

Solar cells were completed with a top contact consisting of LiF (1 nm) and Al (100 nm) deposited by vacuum evaporation at $\approx 3 \times 10^{-7}$ mbar. The active area of the cells was 0.091 cm^2. *J-V* characteristics were measured under ≈100 mW/cm^2 white light from a tungsten-halogen lamp filtered by a Schott GG385 UV filter and a Hoya LB120 daylight filter, using a Keithley 2400 source meter. The mismatch factor of this lamp to the AM1.5 (100 mW/cm^2) spectrum was not determined (see Table I for the device parameters). *J-V* data for the solar cells analyzed with impedance spectroscopy are listed in the Supplemental Material.[17]

B. Impedance spectroscopy measurements

Impedance spectroscopy was performed using a Solartron 1260 impedance analyzer. White light steady-state illumination was obtained from a tungsten-halogen lamp filtered by a Schott GG385 UV filter and a Hoya LB120 daylight filter,

TABLE I. Solar cells characteristics: short-circuit current (J_{sc}), open-circuit voltage (V_{oc}), fill factor (*FF*), and maximum power point (*MPP*) under 100 mW/cm^2 illumination.

Solar cell	J_{sc}(mA/cm^2)	V_{oc}(V)	*FF*	*MPP*(mW/cm^2)
P3HT[60]: PCBM as-cast	4.13	0.62	0.6	1.53
P3HT[60]: PCBM annealed	7.94	0.54	0.69	2.96
MDMO-PPV: [70]PCBM	3.11	0.84	0.55	1.44
PCPDTBT: [70]PCBM	9.06	0.67	0.42	2.55

TABLE II. An overview of the parameters that were used in the model to simulate the P3HT:[60]PCBM cell incorporating the Al_2O_3 layer.

Property	Value	Unit
LUMO energy	4.1	eV
HOMO energy	5.2	eV
LUMO DOS	0.3	nm^{-3}
HOMO DOS	0.3	nm^{-3}
Electron mobility	1×10^{-7}	$m^2V^{-1}s^{-1}$
Hole mobility	1×10^{-7}	$m^2V^{-1}s^{-1}$
Relative dielectric constant	3.6	-
Generation rate	10	$nm^{-3}s^{-1}$
Injection barrier	0.2	eV
Recombination prefactor R	0.1	-

achieving 100 mW/cm^2. Impedance measurements were done under inert conditions (O_2, $H_2O \lesssim 1$ ppm) on freshly prepared devices.

C. Numerical modeling

A one-dimensional numerical model was used to reproduce the experimental results of the structure containing the insulating Al_2O_3 layer. An active layer of length $L = 70$ nm was divided in $N = 36$ discrete points that represented the P3HT:PCBM layer. The relative dielectric constant was set at 3.6. The insulating layer with dielectric constant of 9.5 was placed next to the active layer. The numerical model solves the drift-diffusion equations and Poisson's equation on this grid by forward integration in time. A detailed description of the numerical model can be found in Ref. 18. Electrons and holes were injected from metal contacts described by a Boltzmann factor ($-E_{\rm inj}/kT$). The hole and electron injection barriers ($E_{\rm inj}$) were set at 0.2 eV. Carriers were generated with a rate g at each grid point in the active layer. The effect of inhomogeneity on the exciton generation was investigated numerically.[17] Nonuniformity in the rate of exciton generation has a rather limited effect on the conductance and capacitance. In the simulation, only bimolecular Langevin-type recombination was considered. In the simulations the rate of recombination γ is taken as $R\gamma_0$ with R an adjustable recombination prefactor and γ_0 the Langevin expression: $\gamma_0 = (q/\varepsilon_0\varepsilon_r)(\mu_p + \mu_n)$. The temperature T was set at 300 K. Table II lists the parameters used in the simulations.

To compute the admittance spectrum, the currents through the diode were first allowed to decay to zero in the modeling procedure. After this, a voltage step of 0.01 V was applied and the resulting step response of the current was calculated. The complex admittance spectra were then derived by a fast Fourier transform of the derivative of the conductance.

III. MODELING

A. Analytical model of charge transport with bimolecular recombination at open circuit

In this section we derive an analytical expression for the capacitance and conductance of a solar cell under open-circuit conditions. To simplify the modeling as much as possible we assume that the positive (p) and negative (n) charge carriers have the same mobility μ and diffusion constant D (i.e., $\mu_n = \mu_p$ and $D_n = D_p$) and that these are related via the Einstein relation. We model the bulk heterojunction as a single homogenous material with effective bands for electron and hole transport. Furthermore we assume spatially homogeneous charge carrier generation with rate g and a homogenous recombination via the Langevin mechanism with recombination rate γnp, in which γ is a constant and n and p are the density of electrons and holes. The generation g is assumed to be independent of the local electric field strength. We restrict ourselves to one dimensional transport of charges in the x direction and include drift and diffusion contributions to the transport. The origin $x = 0$ is chosen in the middle of the bulk heterojunction layer with thickness L.

Under these approximations the following differential equations for the electron (n) and hole (p) carrier density apply in the bulk of the material:

$$p'' - \frac{F}{V_T}p' - \frac{F'}{V_T}p - \frac{\gamma}{D}np + \frac{g}{D} = \frac{1}{D}\frac{\partial p}{\partial t} \tag{1}$$

$$n'' + \frac{F}{V_T}n' + \frac{F'}{V_T}n - \frac{\gamma}{D}np + \frac{g}{D} = \frac{1}{D}\frac{\partial n}{\partial t}, \tag{2}$$

where the prime indicates d/dx and the double prime d^2/dx^2. Further, $V_T = kT/q$ is the thermal voltage and F the electric field strength. F is a scalar related to the electrostatic potential $\varphi(x) : F(x) = -\varphi(x)'$.

To make optimal use of the symmetry relation in charge carrier transport we introduce the total carrier density $Q = p + n$ and the net charge density $M = p - n$ as alternatives for p and n. Making use of symmetry, it suffices to solve the second-order differential equation for M

$$M'' - \frac{F}{V_T}Q' - \frac{F'}{V_T}Q = \frac{1}{D}\frac{\partial M}{\partial t}. \tag{3}$$

This equation can be simplified by neglecting the term containing Q'. This approximation can be related to an approximation that is often used in charge transport: the linearization of the Poisson-Boltzmann equation. This linearization is used in, e.g., Debye-Hückel theory for conduction in electrolytes and the second derivative of the potential is expressed in terms of the potential itself,[19]

$$\varphi'' = \kappa^2\varphi = \frac{\tilde{q}}{V_T}Q\varphi, \tag{4}$$

where $\tilde{q} = q/\varepsilon_0\varepsilon_r$. To show how the linearization of the Poisson-Boltzmann relates to the magnitude of the $(F/V_T)Q'$ term in (3) we first combine (4) with the Poisson equation $F' = \tilde{q}M$. This gives

$$Q(x)\frac{\varphi(x)}{V_T} = -M(x). \tag{5}$$

Considering that the diode is under open-circuit condition ($J_p + J_n = 0$ under steady state) gives

$$M' - \frac{F}{V_T}Q = 0. \tag{6}$$

So that

$$M' = -Q'\frac{\varphi}{V_T} - Q\frac{\varphi'}{V_T} = Q'\frac{\varphi}{V_T} + Q\frac{F}{V_T} = \frac{F}{V_T}Q. \quad (7)$$

It follows thus that $Q'(\varphi/V_T) = 0$. In the case where φ is not constant and not equal to zero, we find that $Q' = 0$. Next we introduce the small signal approximation. In impedance spectroscopy a small alternating voltage is applied around the constant open-circuit voltage φ_0 so

$$\varphi(t) = \varphi_0 + \varphi_1(t) = \varphi_0 + \varphi_1 e^{i\omega t}. \quad (8)$$

Adopting the usual small signal analysis we get

$$M = M_0 + M_1(t) = M_0 + M_1 e^{i\omega t} \quad (9)$$

and a corresponding relation for Q. The admittance of the diode can now be evaluated by calculating the ac current density J_1 exactly in the middle of the diode at $x = 0$ where $M_0 = 0$. This gives the following second-order differential equation for M_1:

$$M_1'' - \frac{\tilde{q}}{V_T}Q_0 M_1 - i\frac{\omega}{D}M_1 = 0. \quad (10)$$

At $x = 0$ the derivative of Q_0 with respect to x vanishes and Q_0 is approximately constant along x with a magnitude depending on the carrier generation rate g. Taking into account the boundary condition $M_1 = 0$ at $x = 0$, the solution to (10) is

$$M_1(x) = a_1 \sinh(\sqrt{[f(g,\omega)]}x), \quad (11)$$

where

$$f(g,\omega) = \frac{\tilde{q}Q_0(g)}{V_T} + i\frac{\omega}{D}. \quad (12)$$

Using the identity $np = (1/4)(Q^2 - M^2)$ and the fact that in the bulk at open circuit the rate of recombination has to match the rate of generation $\gamma np = g$, we get at $x = 0$

$$Q_0(g) = \sqrt{\frac{4g}{\gamma} + {M_0}^2(x)} \cong \sqrt{\frac{4g}{\gamma}}. \quad (13)$$

The amplitude a_1 in Eq. (11) depends on the applied voltage because

$$-\varphi_1 = \iint F_1' = \tilde{q}\iint M_1. \quad (14)$$

Using (11) we get

$$a_1 = \frac{-\varphi_1 f(g,\omega)}{\sinh\left(\sqrt{f(g,\omega)}\frac{L}{2}\right)} \quad (15)$$

so that the final expression for M_1 near $x = 0$ is

$$M_1 = \frac{-\varphi_1 f(g,\omega)}{\sinh\left(\sqrt{f(g,\omega)}\frac{L}{2}\right)}\sinh(\sqrt{f(g,\omega)}x). \quad (16)$$

The measured current density in an ac impedance measurement includes a contribution from the displacement current. The measured current density J_{meas} is related to the particle current density and the displacement $\mathcal{D}$ in the following way:

$$J_{\text{meas}} = J + \frac{1}{q_e}\frac{\partial \mathcal{D}}{\partial t} = J + \frac{\varepsilon_0\varepsilon_r}{q_e}\frac{\partial F}{\partial t} = J + \frac{1}{\tilde{q}}\frac{\partial F}{\partial t}. \quad (17)$$

The measured current density is constant throughout the diode and hence the admittance derived at $x = 0$ should hold for the diode as a whole. The measured ac current density in the diode can now be expressed as

$$J_{\text{meas},1}/D = J_1/D + \frac{i\omega}{\tilde{q}D}F_1 = \left(n' + \frac{F}{V_T}n\right) - \left(p' - \frac{F}{V_T}p\right) + \frac{i\omega}{\tilde{q}D}F_1, \quad (18)$$

$$J_{\text{meas},1}/D = -{M_1}' + \frac{F_1 Q_0}{V_T} + \frac{F_0 Q_1}{V_T} + \frac{i\omega}{\tilde{q}D}F_1 = -{M_1}' + f(g,\omega)F_1 + \frac{F_0 Q_1}{V_T}. \quad (19)$$

From small signal analysis of $np = (1/4)(Q^2 - M^2)$ it follows that

$$Q_0 Q_1 - M_1 M_0 = 0. \quad (20)$$

At $x = 0$, $M_1 = 0$ because of symmetry and therefore also $Q_1 = 0$. This gives

$$J_{\text{meas},1}(x = 0)/D = -{M_1}'(0) + f(g,\omega)\int M_1. \quad (21)$$

The ac admittance of the diode becomes

$$Y(\omega) \equiv G(\omega) + i\omega C(\omega) = \frac{J_{\text{meas},1}(x = 0)}{\varphi_1} = \frac{D(-{M_1}'(0) + f(g,\omega)\int M_1)}{\varphi_1}. \quad (22)$$

We need

$${M_1}'(x = 0)$$

and

$$f(g,\omega)\int_{-L/2}^{x=0} M_1$$

to obtain Y(ω). From (16)

$${M_1}'(x = 0) = \frac{-\varphi_1 f^{3/2}(g,\omega)\cosh(0)}{\sinh\left(\sqrt{f(g,\omega)}\frac{L}{2}\right)} = \frac{-\varphi_1 f^{3/2}(g,\omega)}{\sinh\left(\sqrt{f(g,\omega)}\frac{L}{2}\right)}. \quad (23)$$

Then

$$f(g,\omega)\int_{-L/2}^{x=0} M_1 = \frac{-\varphi_1 f^{3/2}(g,\omega)}{\sinh\left(\sqrt{f(g,\omega)}\frac{L}{2}\right)}\cosh(\sqrt{f(g,\omega)}x)\Big|_{x=-L/2}^{x=0} = -\frac{\varphi_1 f^{3/2}(g,\omega)}{\sinh\left(\sqrt{f(g,\omega)}\frac{L}{2}\right)} + \frac{\varphi_1 f^{3/2}(g,\omega)}{\tanh\left(\sqrt{f(g,\omega)}\frac{L}{2}\right)}. \quad (24)$$

Inserting (23) and (24) into (22), we get

$$Y(g,\omega) = \frac{D f^{3/2}(g,\omega)}{\tanh\left(\sqrt{f(g,\omega)}\frac{L}{2}\right)}. \quad (25)$$

At sufficiently high intensity, the nominator in (25) containing the hyperbolic tangent approaches unity so that at low

frequency

$$G(g) = D\left(\frac{\tilde{q}}{V_T}\right)^{3/2}\left(\frac{g}{\gamma}\right)^{3/4}, \tag{26}$$

$$C(g) = \frac{3}{2}\left(\frac{\tilde{q}}{V_T}\right)^{1/2}\left(\frac{g}{\gamma}\right)^{1/4}. \tag{27}$$

Equations (26) and (27) are essentially the zero- and first-order terms from a Taylor expansion of (25) in ω around $\omega = 0$. The accuracy of the approximations (26) and (27) can be checked numerically. Using the parameters from Table II and an active layer thickness L of 100 nm, we find that at a frequency of 10^5 Hz, the relative error in the capacitance as expressed by (27) is less than 5% for illumination intensities exceeding 0.001 sun. The relative error in the conductance (26) at 10^5 Hz is less than 0.05 for intensities above 0.01 sun.

We note that by taking the ratio between capacitance and conductance one obtains a characteristic time τ (often interpreted as minority carrier lifetime). Using the Langevin-type expression (28) for γ with adjustable prefactor R

$$\gamma = R\tilde{q}2\mu, \tag{28}$$

one finds

$$\frac{C(g)}{G(g)} = \tau(g) = \left(\frac{3V_T}{2\tilde{q}D}\right)\left(\frac{g}{\gamma}\right)^{-1/2} = \sqrt{\left(\frac{9R}{2\tilde{q}\mu}\right)}\,\frac{1}{\sqrt{g}}. \tag{29}$$

B. Space-charge-limited current in photovoltaic diodes

The results obtained in the previous section can qualitatively be related to the better known behavior under static conditions. Photovoltaic diodes may, under certain conditions, generate a photocurrent that is limited by the maximum allowed space charge inside the diode.[12,13] In this space-charge-limited operating condition, the dependence of photocurrent on the generation rate g follows a power law with exponent 3/4

$$J_{ph} = q\left(\frac{9\varepsilon_0\varepsilon_r\mu}{8q}\right)^{1/4} g^{3/4}V^{1/2}. \tag{30}$$

The similarity in the dependence on generation rate in the expressions (26) for the conductance and (30) for the steady-state photocurrent, suggests that the intensity dependence of the conductance expressed by relation (26) may be understood in terms of a space-charge limitation on the ac photocurrent. In (26), because in the derivation the electrodes were not taken into account explicitly, charge extraction or injection cannot be limiting the current. Also charge generation was assumed to occur with unit efficiency after photon absorption. As mentioned in the introduction, the concept of space-charge-limited photocurrents presupposes a bulk recombination mechanism. Hence the ac currents near open-circuit conditions as considered in the derivation of (26) must be limited by a combination of restrictions on the buildup of space charge and kinetic limitations imposed by the bimolecular Langevin-type recombination of charge carriers.

As pointed out by Goodman and Rose[12] the thickness l of the space-charge region that limits the current scales with the generation rate to the inverse 1/4 power

$$l = \left(\frac{9\varepsilon_0\varepsilon_r\mu}{8qg}\right)^{1/4} V^{1/2}. \tag{31}$$

If we assume that the capacitance scales with the inverse thickness of the current limiting layer, it follows that space-charge-limited photocapacitance varies with generation rate to the 1/4 power,[20] consistently with the finding of Eq. (27). As an alternative but equivalent reasoning we can consider that in open-circuit conditions all charge carriers recombine, either in the bulk or, after diffusion, at the electrodes. Under conditions of high illumination intensity and negligible electrode- and trap-mediated recombination, the bimolecular Langevin recombination mechanism predicts a lifetime τ for photogenerated carriers that varies as $g^{-1/2}$.[21] Using the relation $C = \tau G$ it follows from (30) that photocapacitance should vary as $g^{1/4}$, consistent with (27) and (31).

C. Diffusion and recombination limited cases

In this section we first examine the limiting case where transport of charge is purely diffusive. Neglecting the terms in Eq. (3) involving the electric field, we get

$$M'' = \frac{1}{D}\frac{\partial M}{\partial t}. \tag{32}$$

This relation implies that M_1 is independent of intensity. Starting from Eq. (21), it then follows that the light dependence of the ac current in the impedance experiment is solely determined by the relation between Q_0 and intensity. For the limiting case of diffusive transport, an expression for Q_0 can be derived starting from Eqs. (1) and (2)

$$Q'' - \frac{F}{V_T}M' - \frac{F'}{V_T}M + -\frac{\gamma}{D}(Q^2 - M^2) + \frac{2G}{D} = \frac{1}{D}\frac{\partial Q}{\partial t} = 0. \tag{33}$$

Neglecting the field-related terms and considering the middle of the device where $M = 0$, one gets

$${Q_0}'' - \frac{\gamma}{D}{Q_0}^2 + \frac{2G}{D} = 0. \tag{34}$$

The general solution to this differential equation (Weierstrass elliptic function $\wp$) can be simplified further by neglecting recombination yielding $Q_0 \propto g$. Sokel and Hughes have applied the same set of approximations for deriving their analytical expression for the photoconductivity.[22] Consistent with their results, we get a conductance G at V_{oc} linear in light intensity and, in addition, capacitance C independent of light intensity.

Equation (34) can also be solved in the limit where transport is negligible compared to recombination, viz. neglecting the Q'' term. In this recombination limited case, one obtains $Q_0 \propto \sqrt{2g/\gamma}$ and so $G \propto \sqrt{I}$ and C independent of light intensity. Thus, analysis of the diffusion and recombination limits indicates that the set of power-law dependencies $G \propto I^{3/4}$ and $C \propto I^{1/4}$ relates specifically to drift-diffusion transport coupled with bimolecular recombination of electron and holes under conditions close to open circuit.

D. Equivalent circuit analysis

The two types of devices under investigation in this study are represented schematically in Fig. 2. Both types of devices may be represented by the equivalent circuit shown on the left of Fig. 2. With the help of this equivalent circuit we now analyze the influence of the probe capacitor C_{probe} on the total admittance. We derive expressions relating the admittance of the bulk heterojunction layer in the solar cell to the total admittance of the photovoltaic diode-probe capacitor combination. The photovoltaic cell is connected in series with a probe capacitor (see Fig. 2). This gives a total admittance

$$\frac{1}{Y_{\text{total}}(\omega)} = \frac{1}{Y_d(\omega)} + \frac{1}{Y_{\text{probe}}(\omega)}. \tag{35}$$

Using

$$Y_{\text{total}}(\omega) = G_{\text{total}}(\omega) + i\omega C_{\text{total}}(\omega)$$
$$Y_d(\omega) = G_d(\omega) + i\omega C_d(\omega)$$

and

$$Y_{\text{probe}}(\omega) = +i\omega C_{\text{probe}}(\omega),$$

C_{total} and G_{total} can be rewritten as

$$C_{\text{total}}(\omega) = C_{\text{probe}} \frac{1 + \omega^2 \frac{C_d}{G_d}\left[\left(\frac{C_d + C_{\text{probe}}}{G_d}\right)\right]}{1 + \omega^2\left[\left(\frac{C_d + C_{\text{probe}}}{G_d}\right)^2\right]} \tag{36}$$

and

$$G_{\text{total}}(\omega) = \frac{\omega^2 C_{\text{probe}}^2 G_d}{G_d^2 + \omega^2 (C_{\text{probe}} + C_d)^2}, \tag{37}$$

which goes from 0 at $\omega = 0$ to G_d in the high-frequency limit, when $C_{\text{probe}} \gg C_d$. Defining

$$\tau_d \equiv \frac{C_d}{G_d}$$

and

$$\tau_{\text{probe}} \equiv \frac{C_{\text{probe}}}{G_d}$$

(36) can be rewritten as

$$C_{\text{total}}(\omega) = C_{\text{probe}} \frac{1}{1 + \omega^2(\tau_d + \tau_{\text{probe}})^2} + C_{\text{probe}} \frac{\omega^2 \tau_d (\tau_d + \tau_{\text{probe}})}{1 + \omega^2(\tau_d + \tau_{\text{probe}})^2}. \tag{38}$$

Provided that $C_{\text{probe}} \gg C_d$, in the high frequency limit this expression reduces to

$$C_{\text{total}}(\omega) \cong C_{\text{probe}} \frac{\tau_d}{(\tau_d + \tau_{\text{probe}})} \cong C_d(\omega) \tag{39}$$

while in the low-frequency limit one obtains

$$C_{\text{total}}(\omega) \cong C_{\text{probe}}. \tag{40}$$

C_d consists of the sum of the geometrical capacitance of the active layer C_{geom} and a light-intensity-dependent term.

The characteristic frequency at which the crossover between high- and low-frequency behavior occurs is

$$\nu_{\text{cross}}(g) = \frac{\omega_{\text{cross}}(g)}{2\pi} \equiv \frac{\sqrt{3}}{6\pi(\tau_d + \tau_{\text{probe}})} \cong \frac{G_d(g)}{2\sqrt{3}\pi C_{\text{probe}}}, \tag{41}$$

where we used $\tau_{\text{probe}} \gg \tau_d$, which follows directly from the assumption $C_{\text{probe}} \gg C_d$. The crossover frequency is defined as the frequency at which the derivative of the capacitance with respect to frequency reaches a maximum.

IV. RESULTS AND DISCUSSION

A. P3HT:[60]PCBM diodes with internal probe capacitor

In Figs. 3(a) and 3(b) the capacitance and conductance for P3HT:[60]PCBM bulk heterojunction diode incorporating a 30-nm thick Al_2O_3 blocking layer are plotted versus ac frequency for different illumination intensities. The layout of the diode is shown in Fig. 2 (top left). An ac amplitude

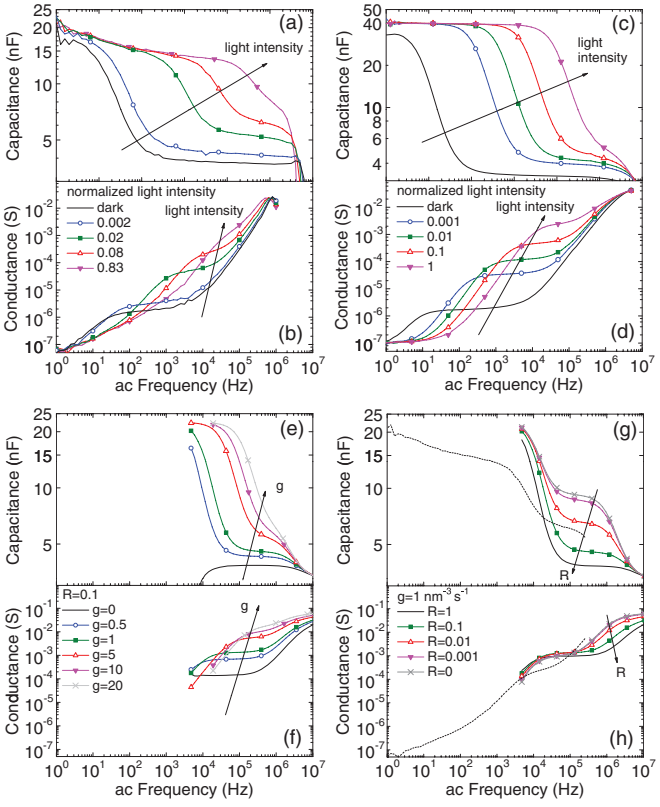

FIG. 3. (Color online) (a), (b) Capacitance and conductance versus ac frequency at different light intensity of as-cast P3HT:[60]PCBM devices containing an Al_2O_3 layer. (c), (d) Same measurements on as-cast P3HT:[60]PCBM devices connected in series to a capacitor. Amplitude of the ac voltage = 50 mV. (e), (f) Simulation of the capacitance and conductance response as a function of ac frequency of a P3HT:[60]PCBM devices containing an Al_2O_3 layer at different generation rates and using a Langevin recombination prefactor R equal to 0.1. (g), (h) Capacitance and conductance were also simulated varying the recombination prefactor for a fixed generation rate $g = 1\ \text{nm}^{-3}\text{s}^{-1}$. The dotted lines in (g), (h) indicate the experimental values for 0.08 Sun intensity.

of 50 mV was used. The blocking Al_2O_3 layer is placed in between the transparent conducting oxide and PEDOT:PSS polymer electrode of the photovoltaic cell. The Al_2O_3 layer is thus sandwiched between quasimetallic layers and not directly in contact with the active bulk heterojunction layer. The geometric capacitance associated with the Al_2O_3 dielectric in between metallic contacts is 20 nF. This is considerably larger that the capacitance estimated for the organic bulk heterojunction layer (3 nF). The Al_2O_3 dielectric incorporated in the photovoltaic diode may therefore be considered as a probe capacitor as discussed in the next section.

We first discuss the response in the dark. In agreement with Eqs. (36) and (38), the capacitance versus ac frequency plots for the diode incorporating the Al_2O_3 layer show three distinct regions. At low frequency the oxide capacitance is dominating (20 nF). This is because the half period of the ac voltage perturbation is long enough to generate and accumulate the amount of charge $Q = C_{\text{probe}}\varphi_1$ needed to fully charge the probe capacitor. At high frequency ($\sim$100 kHz), the half period of the ac modulation is too short in comparison with the carrier transport and generation to fully charge the probe capacitor. In the high-frequency limit, the total capacitance becomes dominated by the active layer geometrical capacitance C_{geom}. The two regions are connected by a transition region centered on the crossover frequency (ν_{cross}) where the capacitance shows a crossover from probe to bulk heterojunction capacitance. At very high frequencies (>500 kHz) the signal is limited by instrumental *RC* times.

Upon increasing the illumination intensity, the crossover frequency shifts to higher values. As anticipated, the 20-nF probe capacitance, observable at low frequency, remains constant with increasing intensity. In contrast, the high-frequency capacitance increases with light intensity. We attribute this to a contribution of photogenerated carriers to the capacitance of the bulk heterojunction layer. The shift of ν_{cross} to higher frequencies with increasing light intensity indicates that the amount of carriers needed to charge the probe capacitor can be generated in a shorter period of time at higher illumination intensity. This indicates significant generation of free charge carriers out of photoexcitations even though the applied potential differs only 50 mV from the open-circuit voltage under this illumination intensity.

Measurements of the conductance also show the same three different frequency regions. At low frequency the conductance is essentially zero due to the blocking of the current by the Al_2O_3 layer. In the transition region, the conductance rises with frequency and reaches a plateau. We call G_{plateau} the conductance measured on the plateau and we assign it to the (photo-)conductance of the bulk heterojunction (G_d in Sec. III C). At very high frequency the conductance rises, which is common for disordered materials and amorphous semiconductors.[23,24] The rise in conductivity at high frequency is also seen in the simulations, in which disorder is ignored. In the simulations the rise in conductivity of a bout two orders of magnitude is a consequence of nonlimiting, i.e., ohmic, contacts on the active layer.[25]

The magnitude of the photoconductance contains information on the efficiency of charge carrier generation. Looking at the highest light intensities, which corresponds roughly to 1 sun intensity, we find $G = 10^{-3}$ S at the plateau near $\nu_{\text{cross}} = 5 \times 10^4$ Hz. The magnitude of G at this frequency combined with the amplitude of the voltage modulation implies a current density on the order of 1 mA/cm^2, which is the same order of magnitude as the short-circuit current density in as-cast P3HT:[60]PCBM cells under AM 1.5 illumination conditions. In addition the $\nu_{\text{cross}} = 5 \times 10^4$ Hz and $C_{\text{probe}} =$ 20 nF also yield current densities on the order of 1 mA/cm^2. Hence the efficiency of charge carrier generation near open-circuit conditions is high. This *a posteriori* justifies the choice for a field-independent charge generation rate g for this device.

B. P3HT:[60]PCBM photovoltaic cell with external probe capacitor

Results for as-cast P3HT:[60]PCBM solar cells connected to an external capacitor (40 nF) are shown in Figs. 3(c) and 3(d). Also in this case, an ac amplitude of 50 mV was used. Taking into account the higher probe capacitance, results are in good agreement with those for the diodes incorporating the Al_2O_3 dielectric current blocking layer. We conclude that the method of incorporating the probe capacitor into the circuit (external or internal) does not significantly influence the results. The method based on the external probe capacitor can be used on standard devices and is therefore preferred.

C. Numerical drift-diffusion modeling of P3HT:PCBM cells

Figures 3(e) and 3(f) show the capacitance and conductance versus ac frequency as predicted from numerical modeling of drift-diffusion processes in the P3HT:PCBM device incorporating the Al_2O_3 and PEDOT:PSS layers. In the simulation, equal electron and hole mobilities were assumed (Table II) and recombination was included using a homogenous Langevin-type mechanism with an adjustable recombination prefactor R. Metallic contacts were taken into account explicitly; relevant band offsets and densities of states are listed in Table II. Figures 3(e) and 3(f) show results for $R =$ 0.1 at different generation rates g. For the P3HT:PCBM cells, $g = 10$ nm^{-3}s^{-1} corresponds approximately to 1 sun illumination intensity. In Figs. 3(g) and 3(h) the photocapacitance and photoconductance are calculated varying the recombination prefactor R at a fixed generation rate $g = 1$ nm^{-3}s^{-1} ($\sim$0.1 sun).

The simulations support the assignment of the low-frequency plateau to the oxide capacitance and the high-frequency plateau to the bulk heterojunction response. The simulations also confirm the rise of the high-frequency capacitance plateau with increasing generation rate. Comparison of Figs. 3(g) and 3(a) leads to an estimate for the recombination prefactor R of about 0.01. The estimation is done identifying the curves that in Figs. 3(g) and 3(h) best match the curves in Figs. 3(a) and 3(b) at 0.08 normalized light intensity. The shift of crossover frequency with increasing rate of carrier generation is also born out.

D. Light-intensity-dependence of the photoconductance and photocapacitance

We now investigate the dependence of the photocapacitance C on illumination intensity in more detail. Values for C are taken from admittance spectra at 100 kHz of the diodes

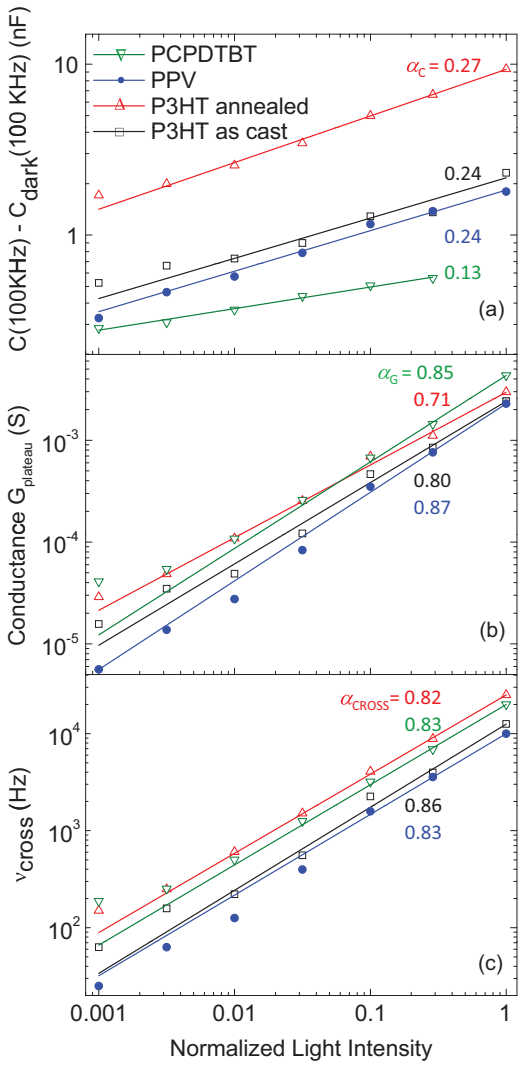

FIG. 4. (Color online) (a) High-frequency capacitance (measured at 100 kHz), (b) conductance $G_{plateau}$, and (c) crossover frequency ν_{cross} measured as a function of light intensity (normalized to 1 sun) on the different solar cells connected in series with the external probe capacitor. The data (symbols) are fitted with a power law I^{α} (lines) in order to extract α_C, α_G, and α_{cross} (see Table III). Black square: P3HT:[60]PCBM as cast, red triangle up: P3HT:[60]PCBM annealed; blue square MDMOPPV:[70]PCBM; green triangle down: P PCPDTBT:[70]PCBM.

with external capacitor [see Figs. 3(c) and 3(d)] and the capacitance in dark at 100 kHz is subtracted. The results are plotted in Fig. 4 as function of light intensity (normalized to 1 sun). Data for as-cast P3HT:[60]PCBM active layers and for three solar cells with other active layers (thermally annealed P3HT:[60]PCBM, MDMO-PPV[70]PCBM, and PCPDTBT:[70]PCBM) are shown.

As can be seen in Fig. 4(a), the dependence of capacitance on intensity I follows a power law I^{α_C}. The exponent α_C obtained from fitting I^{α_C} to the experimental data points amounts to 0.24 for P3HT:[60]PCBM as-cast solar cells. The value $\alpha_C = 0.24$ is in close agreement with the prediction from Eq. (27) $\alpha_C = 1/4$. In Table III values for α_C obtained for different solar cells are listed. Drift-diffusion numerical modeling

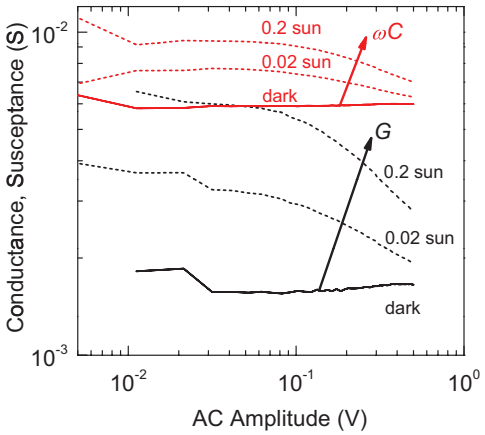

FIG. 5. (Color online) Conductance G and susceptance ωC on the as-cast P3HT:[60]PCBM device incorporating the Al_2O_3 layer as function of the amplitude of the ac voltage at a modulation frequency of 250 kHz. Measurements in dark and at different light intensities are shown.

indicates a power-law dependence and predicts $\alpha_C = 0.4$ for the P3HT:[60]PCBM device incorporating the Al_2O_3 layer, while the experimental value amounts to $\alpha_C = 0.28$.

The $\alpha_C = 0.13$ for the PCPDTBT:[70]PCBM bulk heterojunction shows the largest deviation from the predicted 1/4. Note that field-dependent charge generation is not taken into account in the analytical and numerical models presented above. For MDMO-PPV and P3HT based solar cells this assumption is supported by experimental indication of weak field dependence of charge generation.[26,27] In PCPDTBT:[70]PCBM cells processed without cosolvent, however, strong geminate recombination has been observed and may cause a stronger field dependence in the charge generation.[28–32] For a diode that is recombination limited one expects at high light intensities current densities proportional to $\sqrt{g}$ and carrier lifetimes τ proportional to $1/\sqrt{g}$. Hence photocapacitance is expected to be small and insensitive to light intensity.

The dependence of the admittance $Y = G + i\omega C$ on the voltage amplitude has been investigated. Results for the P3HT:[60]PCBM cell with internal capacitor are shown in Fig. 5. The conductance G in dark probed at 250 kHz (Fig. 5), does not show any significant dependence on ac voltage amplitude; under illumination the conductance decreases with increasing ac amplitude as expected for space-charge-limited conductance and capacitance [see Eqs. (30) and (31)]. The susceptance, ωC, shows a similar dependence of ac voltage amplitude.

Also the intensity dependence of photoconductance has been investigated in more detail. Figure 4(b) shows $G_{plateau}$, the conductance measured on the plateau occurring at the ac frequencies where the capacitance shows a crossover. For example, in P3HT:[60]PCBM devices under 0.01 sun illumination [Figs. 3(c) and 3(d)], this plateau occurs between 10^3 and 10^4 Hz ac frequencies. We find for the as-cast P3HT:[60]PCBM cell with external capacitor that G follows a power-law dependence on intensity with exponent $\alpha_G = 0.80$ (see Table III). Equation (26) predicts $\alpha_G = 3/4$. For the other bulk heterojunctions we find α_G values close to 0.8

TABLE III. Values for α_C, α_G, and α_{cross} relative to the solar cells connected in series with the probe capacitor and to the device containing the Al_2O_3 oxide insulating layer (both measured and simulated).

Solar cell	α_C	α_G	α_{cross}
Experimental			
P3HT:[60]PCBM + oxide as-cast	0.28 ± 0.01	0.81 ± 0.03	0.99 ± 0.03
P3HT:[60]PCBM as-cast	0.24 ± 0.03	0.80 ± 0.03	0.86 ± 0.04
P3HT:[60]PCBM annealed	0.27 ± 0.01	0.71 ± 0.03	0.82 ± 0.01
MDMO-PPV:[70]PCBM	0.24 ± 0.01	0.87 ± 0.02	0.83 ± 0.02
PCPDTBT:[70]PCBM	0.13 ± 0.01	0.85 ± 0.02	0.83 ± 0.01
Simulated[a]			
P3HT:[60]PCBM + oxide, $R = 0.1$	0.42 ± 0.04	0.84 ± 0.02	0.87 ± 0.02

[a]Capacitance evaluated at 950 kHz.

while numerical modeling yields $\alpha_G = 0.84$. For as-cast and annealed P3HT:[60]PCBM cells, the quasistatic conduction G at V_{oc} obtained from quasistatic J-V measurements also follows the $I^{3/4}$ intensity dependence,[17] providing further experimental evidence for space-charge limitation. Additional, indirect indications for space-charge limitation combined with bimolecular recombination, come from the observation that the analytical expression for the photocurrent derived by Sokel and Hughes[22] neglecting space charge and recombination does not give an accurate description of the experimental data.[17]

The crossover frequency ν_{cross} is expected to show the same dependence on light intensity as the high-frequency conductance G according to Eq. (41). Indeed for ν_{cross} we also find a power-law dependence with an exponent ν_{cross} that is similar in magnitude to α_G [see Fig. 3(c) and Table III]. For the P3HT;[60]PCBM bulk heterojunction with internal probe capacitor we find a slightly larger value for ν_{cross}. We expect that in this case nonideal behavior of the thin dielectric in the form of a frequency-dependent leakage and/or C_{probe} may affect the measurement.

Earlier reports on photoadmittance spectroscopy on polymer:fullerene bulk heterojunction solar cells[33,34] report values for α_C and α_G very similar to ours. In these studies open-circuit conditions were imposed by applying a compensating dc bias voltage. In these studies, values for the exponents α_C and α_G were related to trapping of charges in a disorder broadened density of states (DOS) resulting in filling of the DOS at high light intensity. Our results do not exclude trapping of charges in a broadened DOS, but indicate the values α_C close to $1/4$ combined with α_G around $3/4$ may be the result of a more general transport phenomenon: space-charge-limited photocurrents in combination with bimolecular recombination.

Curiously, the intensity dependence of photoadmittance of silver chloride layers can also be described by power laws with exponents $\alpha_C \cong 1/4$ and $\alpha_G \cong 3/4$.[35] In contrast, photocapacitance in inorganic silicon solar cells shows a much more pronounced intensity dependence with $\alpha_C = 1$ at low light intensities.[36,37] At high light intensity α_C can rise above 1 and up to 2.[38]

V. CONCLUSION

We measured the ac (photo-)admittance of polymer:fullerene bulk heterojunction solar cells under conditions close to open-circuit voltage, as function of oscillating bias voltage frequency and illumination intensity for a devices comprising different electron donating polymers blended with PCBM as acceptor. Open-circuit voltage conditions were imposed by incorporating an insulating layer in the solar cell layers stack or, equivalently, by connecting the devices in series with an external capacitor. In the case of the internal oxide layer, the experimental results were reproduced by numerical drift-diffusion simulations including Langevin-type bimolecular recombination of charge carriers. By reproducing the experimental results with the numerical simulations it was possible to estimate the Langevin recombination prefactor R.

We further developed an analytical description of the ac admittance of organic solar cells at open-circuit voltage conditions. We found that at low modulation frequency and at V_{oc} conditions, the capacitance and conductance are expected to vary with illumination intensity I as $C(I) \propto I^{1/4}$ and $G(I) \propto I^{3/4}$ respectively, when bimolecular recombination is taken into account. These dependencies are interpreted in terms of space-charge limitation of the photogenerated current close to open-circuit conditions. We note that the magnitude of the space-charge-limited current vanishes at V_{oc} and for voltages further away from V_{oc}. This implies that as long as there is a small but nonvanishing charge generation rate under open circuit conditions, the current close to V_{oc} should be limited by space-charge consideration. A number of mechanisms for charge carrier generation in disordered organic semiconductors predict a small probability for charge generation under zero applied electric field.[39–41] For applied bias voltages further away from V_{oc} there is the possibility that the current is no longer limited by space-charge considerations but by other factors such as, e.g., charge generation. Therefore the space-charge limitation found here near V_{oc} does not necessarily contradict evidence for field-dependent carrier generation as current limiting factor as reported for, e.g., MDMO-PPV:[60]PCBM at higher bias.[9,42]

An open question in the analysis and modeling is the possible influence of a difference in mobility for electrons and holes on the intensity dependencies predicted. For instance, for MDMO-PPV:[60]PCBM there is experimental evidence for such a difference in electron and hole mobility, amounting to an order of magnitude.[43] We investigated the dependence of conductance and capacitance of our devices on light intensity and established a power-law-type dependency near open-circuit conditions. The exponents observed are consistent with predictions for space-charge-limited photocurrent in

the bulk heterojunction layers. Only PCPDTBT:[70]PCBM based devices processed without cosolvent, showed a weaker dependence of capacitance on the light intensity, indicating that space-charge limitation was not reached in that case. Note that this conclusion will most likely not apply to PCPDTBT:[70]PCBM layers that are fully optimized using cosolvent processing.

To conclude we suggest that close to open-circuit conditions, the photocurrent in organic solar cells can be limited by the buildup of space charge. Space-charge-limited conditions are more likely to be reached by solar cells for which free charge generation is only weakly dependent on electric field and occurs with high efficiency. For active layers in which the photogeneration of current is strongly limited by geminate recombination, such as in PCPDTBT:PCBM, the space-charge limit might not be reached.

Our results indicate that relatively well-performing polymer solar cells can still be limited in fill factor by space-charge effects. In such case, options to increase the fill factor would be the enhancement of the charge carrier mobility or the suppression of Langevin recombination and lowering of R by, e.g., reducing the interfacial area between donor and acceptor phase in the bulk heterojunction.

ACKNOWLEDGMENTS

The work of D.D.N. forms part of the research program of the Dutch Polymer Institute (DPI, Project 631). We thank Kevin van den Ruit for useful suggestions for improvements in the experiments and Christian Helvoirt for the deposition of the Al_2O_3 layers.

*s.c.j.meskers@tue.nl

[1] R. F. Service, Science **332**, 293 (2011).
[2] M. A. Green, K. Emery, Y. Hishikawa, W. Warta, and E. D. Dunlop, Prog. Photovoltaics **20**, 606 (2012).
[3] Y. Y. Liang, Z. Xu, J. B. Xia, S. T. Tsai, Y. Wu, G. Li, C. Ray, and L. P. Yu, Adv. Mater. **22**, E135 (2010).
[4] Z. C. He, C. M. Zhong, X. Huang, W. Y. Wong, H. B. Wu, L. W. Chen, S. J. Su, and Y. Cao, Adv. Mater. **23**, 4636 (2011).
[5] Z. C. He, C. M. Zhong, S. J. Su, M. Xu, H. B. Wu, and Y. Cao, Nature Photon. **6**, 591 (2012).
[6] G. Li, R. Zhu, and Y. Yang, Nature Photon. **6**, 153 (2012).
[7] L. T. Dou, J. B. You, J. Yang, C. C. Chen, Y. J. He, S. Murase, T. Moriarty, K. Emery, G. Li, and Y. Yang, Nature Photon. **6**, 180 (2012).
[8] T. M. Clarke and J. R. Durrant, Chem. Rev. **110**, 6736 (2010).
[9] V. D. Mihailetchi, L. J. A. Koster, J. C. Hummelen, and P. W. M. Blom, Phys. Rev. Lett. **93**, 216601 (2004).
[10] S. R. Cowan, A. Roy, and A. J. Heeger, Phys. Rev. B **82**, 245207 (2010).
[11] S. M. Sze and K. K. Ng, *Physics of Semiconductor Devices* (Wiley-Interscience, Chichester, 2007).
[12] A. M. Goodman and A. Rose, J. Appl. Phys. **42**, 2823 (1971).
[13] V. D. Mihailetchi, J. Wildeman, and P. W. M. Blom, Phys. Rev. Lett. **94**, 126602 (2005).
[14] R. Kern, R. Sastrawan, J. Ferber, R. Stangl, and J. Luther, Electrochim. Acta **47**, 4213 (2002).
[15] M. Adachi, M. Sakamoto, J. T. Jiu, Y. Ogata, and S. Isoda, J. Phys. Chem. B **110**, 13872 (2006).
[16] P. P. Boix, A. Guerrero, L. F. Marchesi, G. Garcia-Belmonte, and J. Bisquert, Adv. Energy Mater. **1**, 1073 (2011).
[17] See Supplemental Material at http://link.aps.org/supplemental/10.1103/PhysRevB.87.085207 for static *I-V* characteristics of solar cells investigated, determination of conductance at open circuit from static current-voltage characteristic for annealed and as-cast P3HT:[60]PCBM, and numerical simulations including inhomogenous generations rates.
[18] S. van Reenen, R. A. J. Janssen, and M. Kemerink, Org. Electron. **12**, 1746 (2011).
[19] D. A. McQuarrie, *Statistical Mechanics* (Harper Collins, New York, 1976).
[20] R. S. Crandall, J. Appl. Phys. **55**, 4418 (1984).
[21] Under these conditions, $j \propto n$, $p \propto \sqrt{g}$ and hence $dn/dt \propto -\gamma np \propto -\gamma n\sqrt{g}$, which leads to an exponential decay for n with time constant $\tau^{-1} \propto \gamma\sqrt{g}$.
[22] R. Sokel, and R. C. Hughes, J. Appl. Phys. **53**, 7414 (1982).
[23] A. K. Jonscher, *Dielectric Relaxation in Solids* (Chelsea Dielectrics Press, London, 1983).
[24] H. Overhof and P. Thomas, *Electronic Transport in Hydrogenated Semiconductors* (Springer-Verlag, Berlin, 1989).
[25] H. H. P. Gommans, M. Kemerink, and W. H. A. Schilders, Phys. Rev. B **72**, 165110 (2005).
[26] J. Lee, K. Vandewal, S. R. Yost, M. E. Bahlke, L. Goris, M. A. Baldo, J. V. Manca, and T. V. Voorhis, J. Am. Chem. Soc. **132**, 11878 (2010).
[27] T. G. J. van der Hofstad, D. D. Nuzzo, M. van den Berg, R. A. J. Janssen, and S. C. J. Meskers, Adv. Energy Mater. **2**, 1095 (2012).
[28] M. Lenes, M. Morana, C. J. Brabec, and P. W. M. Blom, Adv. Funct. Mater. **19**, 1106 (2009).
[29] D. J. D. Moet, M. Lenes, M. Morana, H. Azimi, C. J. Brabec, and P. W. M. Blom, Appl. Phys. Lett. **96**, 213506 (2010).
[30] M. Morana, H. Azimi, G. Dennler, H. J. Egelhaaf, M. Scharber, K. Forberich, J. Hauch, R. Gaudiana, D. Waller, Z. H. Zhu *et al.*, Adv. Funct. Mater. **20**, 1180 (2010).
[31] D. Di Nuzzo, A. Aguirre, M. Shahid, V. S. Gevaerts, S. C. J. Meskers, and R. A. J. Janssen, Adv. Mater. **22**, 4321 (2010).
[32] S. Albrecht, W. Schindler, J. Kurpiers, J. Kniepert, J. Blakesley, I. Dumsch, S. Allard, K. Fostiropoulos, U. Scherf, and D. Neher, J. Phys. Chem. Lett. **3**, 640 (2012).
[33] J. Bisquert and G. Garcia-Belmonte, J. Phys. Chem. Lett. **2**, 1950 (2011).
[34] P. P. Boix, M. M. Wienk, R. A. J. Janssen, and G. Garcia-Belmonte, J. Phys. Chem. C **115**, 15075 (2011).
[35] D. A. Wiegand, Phys. Rev. **124**, 104 (1961).
[36] R. S. Crandall, Appl. Phys. Lett. **42**, 451 (1983).

[37]C. Munakata and N. Honma, Jpn. J. Appl. Phys. **26**, 564 (1987).
[38]I. S. Yahia, F. Yakuphanoglu, and O. A. Azim, Sol. Energ. Mat. Sol. C **95**, 2598 (2011).
[39]K. Falkowski, W. Stampor, P. Grygiel, and W. Tomaszewicz, Chem. Phys. **392**, 122 (2012).
[40]C. L. Braun, J. Chem. Phys. **80**, 4157 (1984).
[41]T. Offermans, S. C. J. Meskers, and R. A. J. Janssen, Chem. Phys. **308**, 125 (2005).
[42]M. Mingebach, S. Walter, V. Dyakonov, and C. Deibel, Appl. Phys. Lett. **100**, 193302 (2012).
[43]C. Melzer, E. Koop, V. Mihailetchi, and P. Blom, Adv. Funct. Mater. **14**, 865 (2004).